

# Deep neural network predicts parameters of quantum many-body Hamiltonians by learning visualized wave-functions

Xinran Ma,<sup>1</sup> Z. C. Tu,<sup>1</sup> and Shi-Ju Ran<sup>2,\*</sup>

<sup>1</sup>*Department of Physics, Beijing Normal University, Beijing 100875, China*

<sup>2</sup>*Department of Physics, Capital Normal University, Beijing 100048, China*

(Dated: December 22, 2024)

In the past decades, methods to solve the ground state given a quantum many-body Hamiltonian have been well established. In this work, we consider an inverse problem and demonstrate that convolutional neural network (CNN) can predict the physical parameters of interacting Hamiltonians, such as coupling strengths and magnetic fields, providing the quantum many-body wave-functions as the ground states. We propose QubismNet that consists of two main parts: the Qubism map that visualizes the ground states (or the purified reduced density matrices) as images, and a CNN that maps the images to the target physical parameters. QubismNet exhibits impressive powers of learning and generalization on several quantum spin models. While the training samples are restricted to the states from certain ranges of the parameters, QubismNet can accurately predict the parameters of the states beyond such training regions. For instance, our results show that QubismNet can predict the magnetic fields near the critical point by learning from the states away from the critical vicinity. Our work provides a data-driven way to infer the Hamiltonians that give the designed ground states, and therefore would benefit the existing and future generations of quantum technologies such as Hamiltonian-based quantum simulations.

## I. INTRODUCTION

Machine learning (ML) has recently been applied to various issues that are difficult using purely the “conventional” approaches in physics (for instance, tensor network [1–3], quantum Monte Carlo [4, 5], and etc.). The successful applications include identifying the classical/quantum phases and topologies without computing order parameters [6–12], predicting physical properties of materials [13–15], efficiently representing non-trivial quantum states [16–19], to name but a few.

Among others, solving the eigenstates, particularly the ground states, of a given quantum many-body Hamiltonian belongs to the central topics in the contemporary physics [20, 21]. The inverse problems, which are of equal significance and practicality, are much less studied due to the lack of valid methods. ML serves as a novel approach that has recently gained certain inspiring successes in such problems [22–25]. In particular, one important issue under hot debate is to access the information of the potentials or interactions by learning from physical data. For instance, Hegde *et al* employed the kernel ridge regression to achieve accurate and transferable predictions of Hamiltonians for a variety of material environments [26]. Li *et al* identified the effective Hamiltonians in magnetic systems and extracted the dominant spin interactions in MnO and TbMnO<sub>3</sub> through multiple linear regression [27]. Sehanobish *et al* proposed the quantum potential neural networks to reconstruct the effective potential given the wave functions [28].

However, most existing works in this direction utilize the regression methods or shallow feed-forward neural networks, which usually possess relative low learning or generalizing powers. In ML, one usually uses deep networks, such as convolutional neural network (CNN) [29, 30], to solve sophis-

ticated problems such as the classifications of real-life images. The excellent learning and generalization abilities of CNN have been widely recognized in numerous applications in computer sciences (c.f. Refs. [31–33] for instance). Very recently, Berthussen *et al* utilized CNN to extract the crystal field Stevens parameters from the thermodynamic data, which illustrates the validity of CNN-based method in deducing physical information [34]. Laanait *et al* use an encoder-decode architecture with convolutional layers to generate the local electron density of material by learning from the diffraction patterns [35]. It is interesting and unexplored whether CNN is capable of solving more challenging issues, including those with the presence of strong correlations and many-body effects.

In this work, the problem we consider is inverse to those of solving the eigenstates of a given Hamiltonian. Suppose the state is given. Our aim is to predict the parameters in the many-body Hamiltonian by training a CNN model, so that the given state is the ground state. Solving such an inverse problem would be meaningful and important for, e.g., designing the Hamiltonian of a quantum annealer to prepare a target state [36]. To this end, we propose QubismNet that consists of two main parts (Figure 1 (a)). The first part is a map to transform the states into images, and the second is a CNN to transform the images to the predictions of the target parameters in the Hamiltonian. The purpose of mapping the states to images is to utilize the superior powers of CNN processing images. Similar idea has been used in Ref. [34], where the thermodynamic data (specific heat and others) are transformed to images by wavelet transformation before being fed to the CNN. The state-image map we use is known as Qubism [37], where the obtained images are of fractals (see some examples in Figure 1 (b)) that can reveal the physical properties of the state.

We benchmark QubismNet on several quantum spin models defined on 1D and 2D lattices. The learning and generalization powers of QubismNet are tested by dividing the sam-

\* Corresponding author. Email: [sjran@cnu.edu.cn](mailto:sjran@cnu.edu.cn)

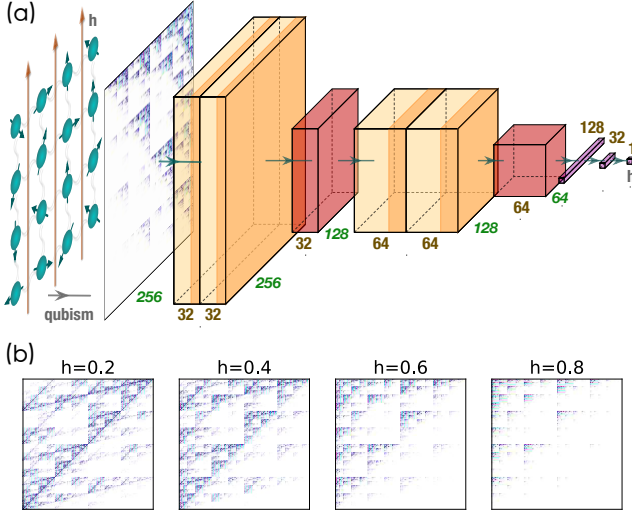


FIG. 1. (Color online) **An illustration for QubismNet, and some sample images of fractals by the Qubism map.** (a) A QubismNet contains two main parts. The first is the Qubism map that transforms a quantum wave-function to an image of fractals. The second is a convolutional neural network that maps the images to the prediction of the target parameters. (b) Examples of the images obtained by Qubism. The ground states are from the XY model with the magnetic fields  $h = 0.2 \sim 0.8$ .

ples (i.e., the ground states taking different values of certain parameter in the Hamiltonian) into testing and generalizing sets. The parameters corresponding to the states in the testing set are independently and identically distributed (*i.i.d.*) as the states in the training set. QubismNet can predict the parameters of such states with high accuracy. The parameters corresponding to the states in the generalizing set are restricted in a certain range in which no training states are taken. Our results show that QubismNet can generalize what it has learned from the training set to predict the parameters of the generalizing states with fair accuracy. For instance, QubismNet only learns from the states away from the critical point and well predicts the magnetic fields given the states in the critical vicinity.

## II. QUBISMNET: PREDICTING PHYSICAL PARAMETERS FROM GROUND STATES

QubismNet consists of two main parts. The first part is a Qubism map [37] that transforms the quantum states to the images of fractals in a one-to-one way. These images are subsequently input to a CNN. The output of the CNN is the physical parameters of the Hamiltonian whose ground states are the input states.

Taking the quantum Ising model (QIM) in a transverse magnetic field as an example, the Hamiltonian reads

$$\hat{H}(h) = J \sum_{\langle i,j \rangle} \hat{S}_i^z \hat{S}_j^z - h \sum_{k=1}^L \hat{S}_k^x, \quad (1)$$

with  $\hat{S}^\alpha$  the  $\alpha$ -component spin operator ( $\alpha = x, z$ ) and  $L$  the system size. Here, we take the coupling constant  $J = 1$  as the energy scale. There are several well-established methods to calculate the ground states given the Hamiltonians, such as density matrix renormalization group (DMRG) [38, 39], tensor network algorithms [1–3], quantum Monte Carlo [4, 5], and etc. This work considers an inverse problem: predicting the magnetic fields  $h$  given the ground states.

In specific, we denote the training set as  $\{|\psi_m\rangle\}$  ( $m = 1, \dots, N_{\text{train}}$ ), where  $|\psi_m\rangle$  is the ground state of  $\hat{H}(h_m)$ . To train the CNN, we choose the mean-square error (MSE) as the loss function

$$\varepsilon = \frac{1}{N_{\text{train}}} \sum_{m=1}^{N_{\text{train}}} (h_m^p - h_m)^2, \quad (2)$$

with  $h_m^p$  the prediction of the magnetic field of  $|\psi_m\rangle$  by the QubismNet. The variational parameters in the CNN are optimized by minimizing the loss function using the gradient method. We choose RMSProp [40] as the optimizer to control the gradient steps. More details of the Qubism map and CNN are provided in the Supplementary Material.

To benchmark the generalization power of QubismNet, we introduce the testing and generalizing sets [41]. The testing sets contains the states whose magnetic fields are different from but *i.i.d.* with the training states. The magnetic fields of the states in the generalizing set are different from both the training and testing states, and are distributed in a different region. For instance, we uniformly choose  $N_{\text{train}}$  values of  $h$  within  $0 < h < 0.5 - \delta/2$  and  $0.5 + \delta/2 < h < 1$  for the training set, and choose other  $N_{\text{test}}$  values of  $h$  in the same regions of  $h$  for the testing set. For the generalizing set, we uniformly choose  $N_g$  values of  $h$  within  $0.5 - \delta/2 < h < 0.5 + \delta/2$ . We dub  $\delta$  as generalization width. Note  $h = 0.5$  is the quantum critical point of QIM. The states in either the testing or the generalizing sets are not fed to the CNN in the training process.

For the large-size systems, it is inefficient to directly apply the Qubism map, as it requires the full coefficients of the quantum states. To avoid such a problem, we bring in the reduced density matrix (RDM) combined with purification. In specific, we choose a subsystem of a moderate size (denoted by  $L_b$ ) and calculate the reduced density matrix  $\hat{\rho}(|\psi_m\rangle) = \text{Tr}_s |\psi_m\rangle\langle\psi_m|$  with  $\text{Tr}_s$  tracing the degrees of freedom in the subsystem. If  $L_b$  is comparable or larger than the correlation length, the RDM would contain the dominant physical information of the whole system [42, 43]. According to our simulations, it is even not necessary to set  $L_b$  larger than the correlation length to accurately predict the physical parameters.

To map a RDM to image by Qubism, we write it as a pure state as  $\hat{\rho}(|\psi_m\rangle) = \sum_{ii'} \rho_{ii'} |i\rangle\langle i'| \rightarrow |\rho_m\rangle = \sum_{ii'} \rho_{ii'} |ii'\rangle$ . One can see that  $|\rho_m\rangle$  is the purification of  $\hat{\rho}(|\psi_m\rangle)^2$  since we have  $\text{Tr}_{i'} |\rho_m\rangle\langle\rho_m| = \hat{\rho}(|\psi_m\rangle)^2$ . Therefore, we feed the QubismNet by  $\{|\rho_m\rangle\}$ , which contain identical amount of information as  $\{\hat{\rho}(|\psi_m\rangle)\}$ . The parameter complexity of  $|\rho_m\rangle$  is independent on the size of the whole system. It is same as the complexity of a state with  $2L_b$  spins.

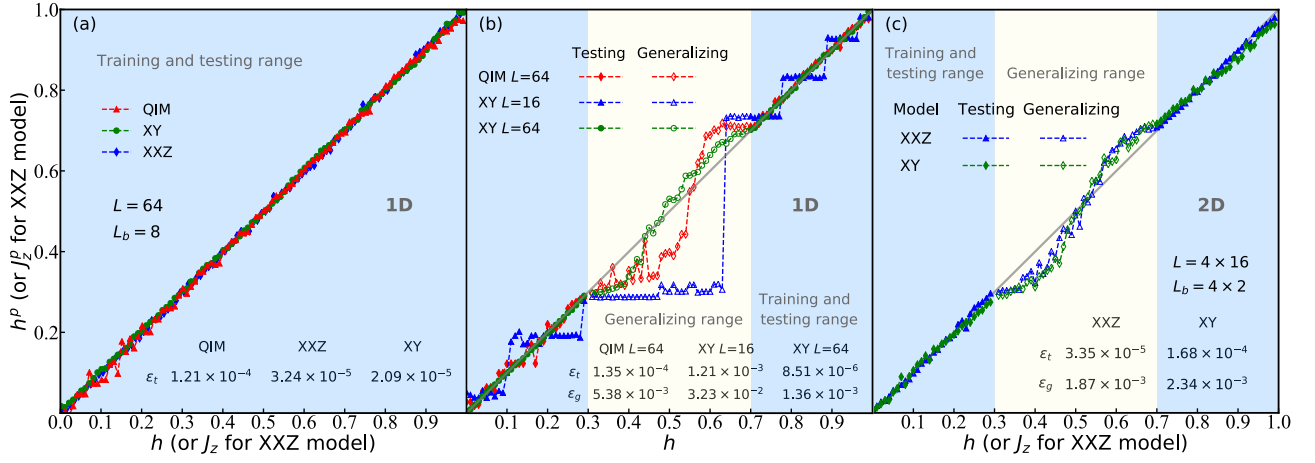


FIG. 2. (Color online) **The predicted parameters of the Hamiltonian ( $h$  or  $J_z$ ) versus the true ones for the QIM, XXZ, and XY models in one and two dimensions.** The blue shadows indicate the ranges of parameters where we take as the training and testing sets. The yellow shadows indicates the range of the generalizing set. The hollow and solid marks give the results of the testing and generalizing sets respectively. The errors of testing and generalizing sets ( $\epsilon_t$  and  $\epsilon_g$ ) can be found in the inset tables. (a) Predictions  $h^p$  or  $J_z^p$  versus the true values  $h$  or  $J_z$  without generalizing set ( $\delta = 0$ ) for the 1D spin models. We take  $L = 64$  with the subsystem size  $L_b = 8$ . The RDM trick is used. (b) Predictions  $h^p$  versus the true  $h$  taking  $\delta = 0.4$  for the 1D spin models. Note the critical point of QIM,  $h = 0.5$ , is put in the middle of the generalizing range. And no RDM trick is used when  $L = 16$  in the XY model. (c) Predictions  $h^p$  versus the true  $h$  for the spin models on a  $4 \times 16$  square lattice.

### III. RESULTS AND DISCUSSIONS

We first benchmark the training and testing accuracies of QubismNet on one-dimensional (1D) QIM by taking  $L = 64$  as the system size and  $L_b = 8$  as the subsystem size in the RDM trick. We take the periodic boundary condition, meaning the first and last spins are interacted as nearest neighbors. Figure 2 (a) shows the predicted fields  $h^p$  against the true fields  $h$ . The  $N_{\text{train}} = 1000$  training states are taken as the ground states by uniformly choosing different magnetic fields in  $0 < h < 1$ . The  $h$ 's of the  $N_{\text{train}} = 100$  testing states are also uniformly taken in  $0 < h < 1$ , which are different from the fields of the training states. No generalizing states are taken (i.e.,  $\delta = 0$ ). The QubismNet accurately predicts the magnetic fields of both the training and testing states. We have the testing accuracy  $\epsilon_t \simeq 1.21 \times 10^{-4}$  evaluated by the loss function, i.e., MSE, of all testing states. The predictions are accurate near the critical point, where the states possess relatively long-range correlations.

We also test the QubismNet on 1D XXZ model with periodic boundary condition. We consider two cases, whose Hamiltonians are written, respectively, as

$$\hat{H}(J_z) = \sum_{\langle i,j \rangle} (\hat{S}_i^x \hat{S}_j^x + \hat{S}_i^y \hat{S}_j^y + J_z \hat{S}_i^z \hat{S}_j^z), \quad (3)$$

$$\hat{H}(h) = \sum_{\langle i,j \rangle} (\hat{S}_i^x \hat{S}_j^x + \hat{S}_i^y \hat{S}_j^y) + h \sum_{k=1}^L \hat{S}_k^z. \quad (4)$$

The physical parameters aimed to predict by the QubismNet are the coupling strength  $J_z$  in Eq. (3) and the longitudinal field  $h$  in Eq. (4). We dub the latter as XY model, where we take zero  $J_z$  and non-zero longitudinal field. We use the RDM

trick with  $L = 64$  and  $L_b = 8$ . The testing accuracies of the XXZ and XY models are about  $\epsilon_t \sim O(10^{-5})$ .

To benchmark the generalization power of QubismNet, we set  $\delta = 0.4$  [Figure 2 (b)]. Within  $0.3 < h < 0.7$  (marked by the light yellow shadow), no training states are taken. In this range, we averagely take  $N_g = 40$   $h$ 's with an interval  $dh = 0.01$  as the generalizing set. For the QIM, a quantum phase transition occurs at  $h = 0.5$ . In our setting, the QubismNet only learns from the states away from the critical vicinity. Our results show that it can generalize from what it has learned and predict the magnetic fields near the critical point. We have the generalizing error (the MSE evaluated by the generalizing set)  $\epsilon_g \sim O(10^{-3})$  using the RDM trick with  $L = 64$  and  $L_b = 8$ .

For the XY and XXZ models, the system is in the gapless phase for  $0 < h < 1$  [44]. For the XY model, we set the same ranges for the training, testing and generalizing sets as above. Without the RDM trick, we take  $L = 16$ , and find that “stages” appear in the  $h$ - $h^p$  curves. This is due to the energy gaps opened by the finite-size effects. For instance, by changing  $h$  of the XY model from 0.15 to 0.28, no energy level crossing occurs. It means the ground states within this range is the same state. Such “stages” obviously hinder the prediction of the physical parameters from the ground states since QubismNet distinguishes no differences from the states by varying  $h$  within a stage. We propose to resolve this issue by increasing  $L$  (e.g., to  $L = 64$ ). The RDM trick has to be used since we cannot handle the full  $2^{64}$  coefficients in the Qubism map. From our results, the “stages” of the  $h$ - $h^p$  curves are largely suppressed using the RDM trick. The testing and generalizing errors are reduced by more than 100 and 20 times, respectively.

We also test on the XXZ and XY models on 2D square lattice with periodic boundary condition. We take the size as

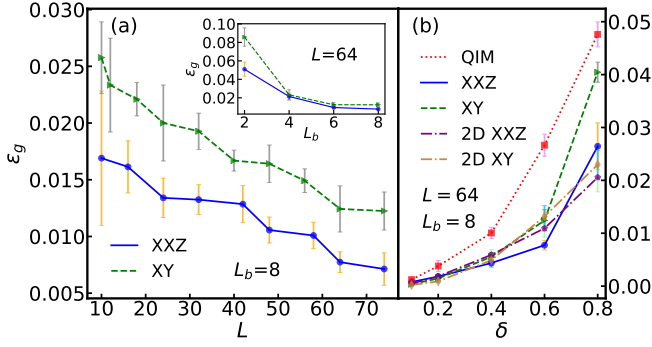


FIG. 3. (Color online) **The errors of the generalizing set  $\epsilon_g$  versus the system size  $L$  and the generalizing width  $\delta$ .** (a) The relation between  $\epsilon_g$  and  $L$  with  $\delta = 0.6$  and  $L_b = 8$  for 1D XXZ and XY models. The inset demonstrates the relation between  $\epsilon_g$  and  $L_b$  with  $L = 64$ . (b) The relation between  $\epsilon_g$  and  $\delta$  for 1D and 2D spin models where we take  $L = 64$  and  $L_b = 8$ .

$4 \times 16$ . The subsystem used to calculate the RDM is chosen in the middle of lattice with the size  $4 \times 2$ . The 2D XY model, whose local Hamiltonian is given by Eq. (4), is in an oscillatory phase for  $0 \leq h \leq 1$ . The XXZ model with its local Hamiltonian given by Eq. (3) is in the paramagnetic phase for  $0 \leq J_z \leq 1$ . In general, 2D quantum models are much more challenging to simulate. QubismNet works well on such 2D quantum systems as shown in Figure 2 (c). With the generalizing width  $\delta = 0.4$ , it gets similar accuracies compared with the one-dimensional systems, with  $\epsilon_t \sim O(10^{-5}) - O(10^{-4})$  and  $\epsilon_g \sim O(10^{-3})$ .

To demonstrate the finite-size effects, we show in Figure 3 (a) the generalizing error  $\epsilon_g$  against  $L$  on the XXZ and XY models ( $\delta = 0.6$ ). The RDM trick is used with  $L_b = 8$ . The error bars here (and all others in this work) are evaluated by independently and randomly taking the initial values of the variational parameters in the CNN for ten times. The  $\epsilon_g$  of both models are still slightly decreasing with  $L$  for  $L > 60$ , meaning it is possible to further reduce the errors by taking larger sizes. In the inset of Figure 3 (a), we fix  $L = 64$  and find that  $\epsilon_g$  well converges as the subsystem size increases to  $L_b > 6$  for the models under consideration. Note it would be inefficient to improve the accuracies by increasing  $L_b$  as the complexity will increase exponentially with it. We have tried larger  $L_b$  and the results indicate little improvement to the accuracies.

In Figure 3 (b), we show  $\epsilon_g$  versus  $\delta$  for the QIM, XXZ, and XY models. We fix  $L = 64$  and use the RDM trick with  $L_b = 8$ . Since the QubismNet only learns from the states sampled in  $0 < h < 0.5 - \delta/2$  and  $0.5 + \delta/2 < h < 1$ , it requires more generalization power to predict the  $h$  of the ground states in  $0.5 - \delta/2 < h < 0.5 + \delta/2$  as  $\delta$  increases. Therefore, the generalizing error  $\epsilon_g$  of the QubismNet monotonously increases with  $\delta$ . But even for  $\delta = 0.8$ , the generalizing error is still insignificant with approximately  $\epsilon_g < 0.05$ . Meanwhile, the predictions become more fluctuated for larger  $\delta$  when randomly initializing the variational parameters of the QubismNet.

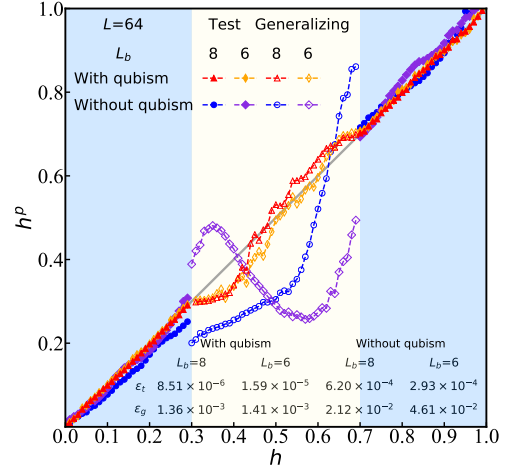


FIG. 4. (Color online) **The prediction  $h^p$  versus the true  $h$  on the 1D XY model ( $L = 64$ ) with and without the Qubism map.** We use the RDM trick with  $L_b = 8$  and  $L_b = 6$ .

In above, we stated that after transforming the states into images, we can take advantage of the superior power of CNN on processing images. Below, we try to directly reshape the coefficients of a RDM into a  $2^{2L_b}$ -dimensional vector. Then we use a 1D version of CNN, which consists of 1D convolutional and pooling layers, to map the vector to the prediction of the target parameters. Figure 4 shows the predictions  $h^p$  versus  $h$  on the 1D XY model with  $L = 64$  and  $L_b = 6$  and 8. The  $\epsilon_t$  and  $\epsilon_g$  without the Qubism map becomes more than ten times larger than that with the Qubism map. These results imply that the Qubism map is a reasonable choice, since the image "visualizes" the physics of the state in the patterns of fractals [37]. We do not exclude the possibilities of other maps that may outperform the Qubism map.

#### IV. SUMMARY AND PERSPECTIVE

It is an open issue if deep neural networks can learn to predict the parameter in a Hamiltonian given the ground states. In this work, we propose QubismNet, which consists of the Qubism Map to transform the quantum states to images, and a CNN to map the images to the prediction of the target physical parameters. We test our proposal on the QIM, XXZ, and XY models in one and two dimensions. QubismNet successfully learns the relations between the states and the parameter, and exhibits impressive learning and generalization powers. Our work shows the feasibility of inferring the Hamiltonians' parameters from states (inverse to the problems of solving the states from Hamiltonians) with the machine learning techniques.

Our work is a start-up of using the classical ML models to directly learn the quantum data (e.g., wave-functions or density matrices) in a different way from the quantum circuit models [45–47]. Our results suggests the impressive learning and generalization powers of CNN in such issues. It could provide a key tool in designing the Hamiltonian in order to,



for instance, prepare target states in Hamiltonian-based quantum simulators [36, 48]. Our proposal can be generalized to learn from the experimental data of quantum measurements in, e.g., a quantum state tomography process [49–51].

## ACKNOWLEDGMENTS

SJR is grateful to Ding Liu and Ya-Tai Miu for helpful discussions. SJR is supported by NSFC (Grant No. 12004266

and No. 11834014), Beijing Natural Science Foundation (No. 1192005 and No. Z180013), Foundation of Beijing Education Committees (No. KM202010028013), and the Academy for Multidisciplinary Studies, Capital Normal University. Z. C. Tu is supported by the National Natural Science Foundation of China (Grant No. 11975050).

- 
- [1] F. Verstraete, V. Murg, and J. I. Cirac, “Matrix product states, projected entangled pair states, and variational renormalization group methods for quantum spin systems,” *Advances in Physics*, vol. 57, no. 2, pp. 143–224, 2008.
  - [2] R. Orús, “Tensor networks for complex quantum systems,” *Nature Reviews Physics*, vol. 1, no. 9, pp. 538–550, 2019.
  - [3] S.-J. Ran, E. Tarrico, C. Peng, X. Chen, L. Tagliacozzo, G. Su, and M. Lewenstein, *Tensor Network Contractions: Methods and Applications to Quantum Many-Body Systems*. Springer Nature, 2020.
  - [4] D. Ceperley and B. Alder, “Quantum monte carlo,” *Science*, vol. 231, no. 4738, pp. 555–560, 1986.
  - [5] M. P. Nightingale and C. J. Umrigar, *Quantum Monte Carlo methods in physics and chemistry*. No. 525, Springer Science & Business Media, 1998.
  - [6] L. Wang, “Discovering phase transitions with unsupervised learning,” *Physical Review B*, vol. 94, no. 19, p. 195105, 2016.
  - [7] J. Carrasquilla and R. G. Melko, “Machine learning phases of matter,” *Nature Physics*, vol. 13, no. 5, pp. 431–434, 2017.
  - [8] E. P. Van Nieuwenburg, Y.-H. Liu, and S. D. Huber, “Learning phase transitions by confusion,” *Nature Physics*, vol. 13, no. 5, pp. 435–439, 2017.
  - [9] P. Zhang, H. Shen, and H. Zhai, “Machine learning topological invariants with neural networks,” *Physical review letters*, vol. 120, no. 6, p. 066401, 2018.
  - [10] B. S. Rem, N. Käming, M. Tarnowski, L. Asteria, N. Fläschner, C. Becker, K. Sengstock, and C. Weitenberg, “Identifying quantum phase transitions using artificial neural networks on experimental data,” *Nature Physics*, vol. 15, no. 9, pp. 917–920, 2019.
  - [11] J. F. Rodriguez-Nieva and M. S. Scheurer, “Identifying topological order through unsupervised machine learning,” *Nature Physics*, vol. 15, no. 8, pp. 790–795, 2019.
  - [12] M. S. Scheurer and R.-J. Slager, “Unsupervised machine learning and band topology,” *Physical Review Letters*, vol. 124, no. 22, p. 226401, 2020.
  - [13] M. Rupp, A. Tkatchenko, K.-R. Müller, and O. A. Von Lilienfeld, “Fast and accurate modeling of molecular atomization energies with machine learning,” *Physical review letters*, vol. 108, no. 5, p. 058301, 2012.
  - [14] T. Xie and J. C. Grossman, “Crystal graph convolutional neural networks for an accurate and interpretable prediction of material properties,” *Physical review letters*, vol. 120, no. 14, p. 145301, 2018.
  - [15] P. Z. Hanakata, E. D. Cubuk, D. K. Campbell, and H. S. Park, “Accelerated search and design of stretchable graphene kirigami using machine learning,” *Physical review letters*, vol. 121, no. 25, p. 255304, 2018.
  - [16] G. Carleo and M. Troyer, “Solving the quantum many-body problem with artificial neural networks,” *Science*, vol. 355, no. 6325, pp. 602–606, 2017.
  - [17] K. Choo, G. Carleo, N. Regnault, and T. Neupert, “Symmetries and many-body excitations with neural-network quantum states,” *Physical review letters*, vol. 121, no. 16, p. 167204, 2018.
  - [18] I. Glasser, N. Pancotti, M. August, I. D. Rodriguez, and J. I. Cirac, “Neural-network quantum states, string-bond states, and chiral topological states,” *Physical Review X*, vol. 8, no. 1, p. 011006, 2018.
  - [19] D.-L. Deng, X. Li, and S. D. Sarma, “Machine learning topological states,” *Physical Review B*, vol. 96, no. 19, p. 195145, 2017.
  - [20] A. Avella, F. Mancini, et al., *Strongly Correlated Systems*. Springer, 2012.
  - [21] Y. Kuramoto, *Quantum Many-Body Physics*. Springer Japan, 2020.
  - [22] R. Fournier, L. Wang, O. V. Yazyev, and Q. Wu, “Artificial neural network approach to the analytic continuation problem,” *Physical Review Letters*, vol. 124, no. 5, p. 056401, 2020.
  - [23] Y. H. Teoh, M. Drygala, R. G. Melko, and R. Islam, “Machine learning design of a trapped-ion quantum spin simulator,” *Quantum Science and Technology*, vol. 5, no. 2, p. 024001, 2020.
  - [24] P. Z. Hanakata, E. D. Cubuk, D. K. Campbell, and H. S. Park, “Forward and inverse design of kirigami via supervised autoencoder,” *Physical Review Research*, vol. 2, no. 4, p. 042006, 2020.
  - [25] L.-F. Arsenault, R. Neuberg, L. A. Hannah, and A. J. Millis, “Projected regression method for solving fredholm integral equations arising in the analytic continuation problem of quantum physics,” *Inverse Problems*, vol. 33, no. 11, p. 115007, 2017.
  - [26] G. Hegde and R. C. Bowen, “Machine-learned approximations to density functional theory hamiltonians,” *Scientific reports*, vol. 7, p. 42669, 2017.
  - [27] X. Li, F. Lou, X. Gong, and H. Xiang, “Constructing realistic effective spin hamiltonians with machine learning approaches,” *New Journal of Physics*, 2020.
  - [28] A. Sehanobish, H. H. Corzo, O. Kara, and D. van Dijk, “Learning potentials of quantum systems using deep neural networks,” *arXiv preprint arXiv:2006.13297*, 2020.
  - [29] Y. LeCun, B. Boser, J. S. Denker, D. Henderson, R. E. Howard, W. Hubbard, and L. D. Jackel, “Backpropagation applied to handwritten zip code recognition,” *Neural computation*, vol. 1, no. 4, pp. 541–551, 1989.
  - [30] A. Krizhevsky, I. Sutskever, and G. E. Hinton, “Imagenet classification with deep convolutional neural networks,” *Communications of the ACM*, vol. 60, no. 6, pp. 84–90, 2017.
  - [31] N. Aloysius and M. Geetha, “A review on deep convolutional neural networks,” in *2017 International Conference on*

- Communication and Signal Processing (ICCSP), pp. 0588–0592, IEEE, 2017.
- [32] G. Yao, T. Lei, and J. Zhong, “A review of convolutional-neural-network-based action recognition,” Pattern Recognition Letters, vol. 118, pp. 14–22, 2019.
- [33] F. Sultana, A. Sufian, and P. Dutta, “A review of object detection models based on convolutional neural network,” in Intelligent Computing: Image Processing Based Applications, pp. 1–16, Springer, 2020.
- [34] N. F. Berthussen, Y. Sizyuk, M. S. Scheurer, and P. P. Orth, “Learning crystal field parameters using convolutional neural networks,” arXiv preprint arXiv:2011.12911, 2020.
- [35] N. Laanait, J. Romero, J. Yin, M. T. Young, S. Treichler, V. Starchenko, A. Borisevich, A. Sergeev, and M. Matheson, “Exascale deep learning for scientific inverse problems,” arXiv preprint arXiv:1909.11150, 2019.
- [36] A. Das and B. K. Chakrabarti, “Quantum annealing and analog quantum computation,” Reviews of Modern Physics, vol. 80, no. 3, p. 1061, 2008.
- [37] J. Rodríguez-Laguna, P. Migdał, M. I. Berganza, M. Lewenstein, and G. Sierra, “Qubism: self-similar visualization of many-body wavefunctions,” New Journal of Physics, vol. 14, no. 5, p. 053028, 2012.
- [38] S. R. White, “Density matrix formulation for quantum renormalization groups,” Physical review letters, vol. 69, no. 19, p. 2863, 1992.
- [39] S. R. White, “Density-matrix algorithms for quantum renormalization groups,” Physical Review B, vol. 48, no. 14, p. 10345, 1993.
- [40] G. Hinton, N. Srivastava, and K. Swersky, “Neural networks for machine learning lecture 6a overview of mini-batch gradient descent,” Cited on, vol. 14, no. 8, 2012.
- [41] Note that the datasets, i.e., the ground states of the Hamiltonians with different physical parameters, are prepared by the exact diagonalization algorithm for small sizes or by DMRG algorithm for large sizes.
- [42] F. Verstraete and J. I. Cirac, “Matrix product states represent ground states faithfully,” Physical Review B, vol. 73, no. 9, p. 094423, 2006.
- [43] V. Zauner, D. Draxler, L. Vanderstraeten, M. Degroote, J. Haegeman, M. M. Rams, V. Stojevic, N. Schuch, and F. Verstraete, “Transfer matrices and excitations with matrix product states,” New Journal of Physics, vol. 17, no. 5, p. 053002, 2015.
- [44] F. Franchini, An introduction to integrable techniques for one-dimensional quantum systems, vol. 940. Springer, 2017.
- [45] K. Mitarai, M. Negoro, M. Kitagawa, and K. Fujii, “Quantum circuit learning,” Physical Review A, vol. 98, no. 3, p. 032309, 2018.
- [46] J.-G. Liu and L. Wang, “Differentiable learning of quantum circuit born machines,” Physical Review A, vol. 98, no. 6, p. 062324, 2018.
- [47] D. Zhu, N. M. Linke, M. Benedetti, K. A. Landsman, N. H. Nguyen, C. H. Alderete, A. Perdomo-Ortiz, N. Korda, A. Garfoot, C. Brecque, et al., “Training of quantum circuits on a hybrid quantum computer,” Science advances, vol. 5, no. 10, p. eaaw9918, 2019.
- [48] I. M. Georgescu, S. Ashhab, and F. Nori, “Quantum simulation,” Reviews of Modern Physics, vol. 86, no. 1, p. 153, 2014.
- [49] K. Vogel and H. Risken, “Determination of quasiprobability distributions in terms of probability distributions for the rotated quadrature phase,” Physical Review A, vol. 40, no. 5, p. 2847, 1989.
- [50] M. Cramer, M. B. Plenio, S. T. Flammia, R. Somma, D. Gross, S. D. Bartlett, O. Landon-Cardinal, D. Poulin, and Y.-K. Liu, “Efficient quantum state tomography,” Nature communications, vol. 1, no. 1, pp. 1–7, 2010.
- [51] B. Lanyon, C. Maier, M. Holzäpfel, T. Baumgratz, C. Hempel, P. Jurcevic, I. Dhand, A. Buyskikh, A. Daley, M. Cramer, et al., “Efficient tomography of a quantum many-body system,” Nature Physics, vol. 13, no. 12, pp. 1158–1162, 2017.

## SUPPLEMENTARY MATERIAL

In the supplementary material, more details about the Qubism map and CNN are provided, and the images obtained by the Qubism map from various models in 1D and 2D are shown. The detailed descriptions on applying QubismNet to 2D quantum systems are given.

### A. Qubism Map

Consider a quantum system with  $L$  spins, denoted by  $s = \{X_1 Y_1 X_2 Y_2 \dots X_{L/2} Y_{L/2}\}$  with  $X_i, Y_i \in \{0, 1\}$ . The resolution of the image obtained by the Qubism map is  $(2^{L/2}, 2^{L/2})$ . Each spin configuration corresponds to the pixel in the  $x$ -th row and  $y$ -th column of the image satisfying

$$\begin{aligned} x &= \sum_{i=1}^{L/2} X_i 2^{(L/2-i)} + 1, \\ y &= \sum_{i=1}^{L/2} Y_i 2^{(L/2-i)} + 1. \end{aligned} \quad (5)$$

The gray-scale value of each pixel is taken as the coefficient of the quantum state in the corresponding spin configuration. Besides, each pixel can be attached to colors based on the phase of quantum state. The images obtained by the Qubism map of 1D QIM, Heisenberg XY, and XXZ models are shown in Figure 5 (a), (b) and (c), respectively. In all these cases, we take  $L = 64$  and  $L_b = 8$ .

### B. Convolutional Neural Network

CNN has shown the superiority in image recognition and many other challenging tasks. In general, CNN consists of several alternative convolutional and pooling layers, which together serve as a feature extractor. One or many fully-connected layers are then used to map the extracted features to the target output in classification and regression. The CNN we use in this work contains eight layers. The first convolutional layer filters the input images with 32 kernels of size  $3 \times 3$  and a stride of size  $1 \times 1$ . The second convolutional layer take the output of the first convolutional layer as input with same setting as the first convolutional layer. The first max-pooling layer of size  $2 \times 2$  follows which downsamples the size of features. Then the third and fourth convolutional layers are used both with 64 kernels of size  $3 \times 3$  and a stride of size  $1 \times 1$ . All convolutional layers use padding around the images so the outputs has the same height/width dimension as the inputs. The second max-pooling layer follows with pool size  $2 \times 2$ . Next, the output of the second max-pooling layer is flattened and then input to two fully-connected layers with 128 and 32 neurons respectively. The output of the last fully connected layer is fed to one neuron which produce the final output of the physical parameter. Note that we choose two successive convolutional layers to improve the quality of features because

of the more complex nonlinearity and larger receptive fields. The rectified linear unit (ReLU) [1, 30] is chosen as activation function for all the convolutional and fully-connected layers. A linear activation function is used for the output layer. The optimizer we use is RMSprop [40] with the initial learning rate 0.001. "He normal initialization" is employed as initialization method which has been proven to get good effect in CNN with the rectifier nonlinearities [2].

Two tricks on avoiding overfitting during the training process is employed. One is the dropout [3, 4] with rate of  $p = 0.5$ , meaning randomly masking 50% of neurons during training. It is a commonly used method making the NN robust. The other is validation. We always save the best model selected by the minimum loss of the validation set which consists of the samples randomly chosen 10% from the training set. The best model is then used on the testing and generalizing set. Note that the input images are normalized so that the features are in  $[0, 1]$ . We construct and train our CNN with Keras [5], a high-level open-source API running on top of TensorFlow. We train the CNN for 300 epochs for each case (one epoch means training by all the samples in training set once). The total training time is roughly 0.3 hours on a server equipped with NVIDIA P100 graphics processing unit when we use 1000 training samples.

Figure 6 (a) shows the loss functions versus epochs for the 1D QIM and XY models with  $L = 64$ ,  $L_b = 8$  and  $\delta = 0.4$ . The loss functions of the training and validation sets decrease rapidly and become quite small in a few epochs for all the three models. This indicates that QubismNet is trainable and feasible. Besides, the validation loss functions do not increase during the whole training process implying no overfitting.

Furthermore, we go deep inside the CNN and see extracted features by the convolutional/pooling part of the CNN. After the last pooling layer, each sample is mapped to a  $64 \times 64 \times 64$  tensor as the extracted features where 64 is the number of channels. Figure 6 (b) shows the average magnitude of each channel  $c$ . We find the the dominant contribution is from the first channel in almost all the cases. In Figure 6 (c), we demonstrate the  $64 \times 64$  features in the first channel. Interestingly, we observe that the prominent features (with larger values marked by the deeper dots) move in general from right to left with the increase of  $h$ . These results indicate that QubismNet capture some consecutive rule from the quantum states in its own way.

### C. RDM-based method for two-dimensional lattice

We follow the standard recipe of DMRG on solving the ground states of 2D quantum models [6]. The 2D lattice model with nearest-neighboring interactions is stretched into a chain with long-range interactions, as illustrated in Figure 7 (a). We set the size of lattice as  $4 \times 16$  for both the 2D XY and XXZ models. The subsystem used to calculate RDM is chosen in the middle of lattice with size  $4 \times 2$  as illustrated. Several images obtained from the ground states of the 2D XY and XXZ models with different  $h$  or  $J_z$  are shown in Figure 7 (b) and (c) as examples.

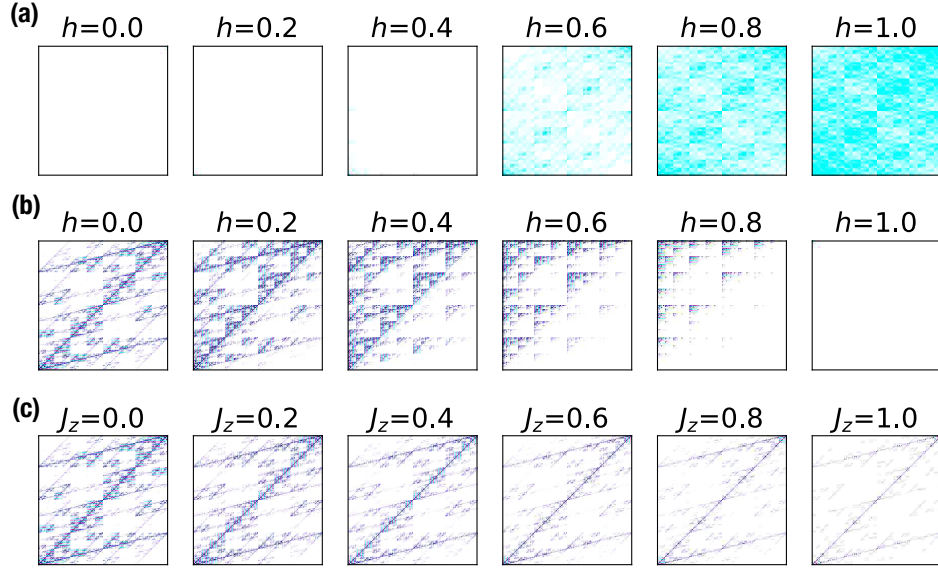


FIG. 5. (Color online) Illustrations of the images by the Qubism map from the ground states of the QIM, XY, and XXZ models.

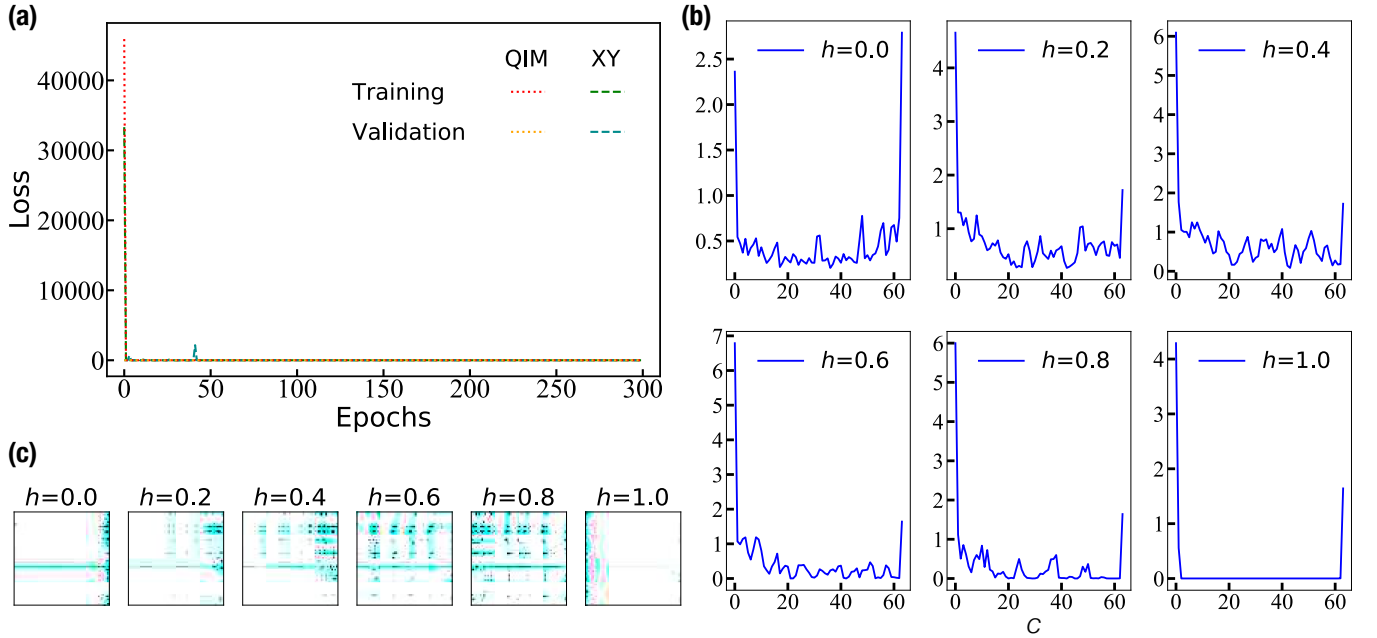


FIG. 6. (Color online) **The loss functions and extracted features of the CNN.** (a) The decreases of the loss function with the training epochs on training and validation set for QIM, XY and XXZ models. (b) For the XY model, we show the average magnitude of the extracted features for different channels  $c$ . For different  $h$ , the dominant contribution is always from the first channel. (c) The extracted  $64 \times 64$  features in the first channel. In general, we observe that the prominent features (illustrated by the dark dots) move from right to left as  $h$  increases.

- [1] Vinod Nair and Geoffrey E Hinton. Rectified linear units improve restricted boltzmann machines. In *ICML*, 2010.
- [2] Kaiming He, Xiangyu Zhang, Shaoqing Ren, and Jian Sun. Delving deep into rectifiers: Surpassing human-level performance on imagenet classification. In *Proceedings of the IEEE international conference on computer vision*, pages 1026–1034, 2015.

- [3] Geoffrey E Hinton, Nitish Srivastava, Alex Krizhevsky, Ilya Sutskever, and Ruslan R Salakhutdinov. Improving neural networks by preventing co-adaptation of feature detectors. *arXiv preprint arXiv:1207.0580*, 2012.



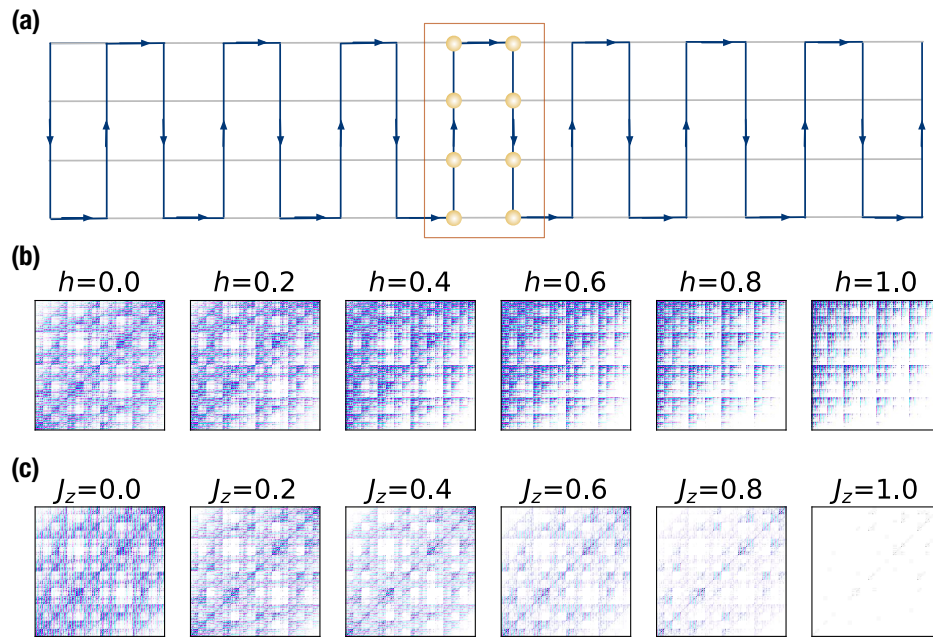


FIG. 7. (Color online) **An illustration of DMRG applied to the 2D system, and the images obtained from the 2D ground states.** (a) An illustration of how the 2D lattice is stretched to a 1D chain in order to use DMRG to simulate the ground states. We choose a  $2 \times 4$  sub-system in the middle to define the RDM. (b) The images obtained by applying the Qubism map to the ground states in the 2D XX model in different transverse fields  $h$ . (c) The images from the 2D XXZ model with different  $J_z$ .

[4] Nitish Srivastava, Geoffrey Hinton, Alex Krizhevsky, Ilya Sutskever, and Ruslan Salakhutdinov. Dropout: a simple way to prevent neural networks from overfitting. The journal of machine learning research, 15(1):1929–1958, 2014.

[5] François Chollet et al. Keras. <https://keras.io>, 2015.  
 [6] Edwin M. Stoudenmire and Steven R. White. Studying two-dimensional systems with the density matrix renormalization group. Ann. Rev. Cond. Matter Phys., 3:111–128, 2012.